Materials Today Chemistry 20 (2021) 100462

Contents lists available at ScienceDirect

Materials Today Chemistry

journal homepage: www.journals.elsevier.com/materials-today-chemistry/

The first representative of a new class of charge transfer complexes in *o*-quinone series for organic semiconductors

E.A. Gusakov [a], O.P. Demidov [b], I.O. Tupaeva [a], E.V. Vetrova [a], M.A. Soldatov [c], A.A. Tereshchenko [c], A.D. Dubonosov [d, *], Y.A. Sayapin [d], A.V. Metelitsa [a], V.I. Minkin [a]

[a] *Institute of Physical and Organic Chemistry, Southern Federal University, Rostov on Don 344090, Russian Federation*
[b] *North-Caucasus Federal University, Stavropol 355017, Russian Federation*
[c] *The Smart Materials Research Institute, Southern Federal University, Rostov on Don 344090, Russian Federation*
[d] *Federal Research Centre the Southern Scientific Centre of the Russian Academy of Sciences, Rostov on Don 344006, Russian Federation*

A R T I C L E I N F O

Article history:
Received 1 December 2020
Received in revised form
14 March 2021
Accepted 16 March 2021
Available online xxx

Keywords:
Charge transfer complex (CT complex)
Organic semiconductor
p-Nitroaniline
[1,10]-Phenanthroline-5,6-dione
X-ray diffraction
Quantum chemical calculations
Band gap

A B S T R A C T

The first representative of a new class of charge transfer complexes for organic semiconductors was synthesized. The reaction of *p*-nitroaniline (PNA) with [1,10]-phenanthroline-5,6-dione (PD) results in the formation of a stable molecular charge transfer (CT) complex PNA_3-PD_2 in a ratio of 3:2. The structure of the molecular CT complex PNA_3-PD_2 was established by X-ray diffraction studies. Using the density functional theory method, it is shown that several types of intermolecular interactions are realized in the complex: between the PNA amino group and the nitro group of another PNA molecule, carbonyl groups, and PD nitrogen atoms. Complex PNA_3-PD_2 is stable only in solid form. The diffuse reflectance UV–vis spectrum of PNA_3-PD_2 crystal powder is characterized by the intense weakly structured long-wavelength absorption band up to 650 nm. Quantum chemical calculations of the electronic structure have shown that the complex PNA_3-PD_2 is a straight-band semiconductor with a band gap of 2.11 eV.

1. Introduction

According to the IUPAC recommendations, charge transfer complex mean an electron-donor–electron-acceptor complex, characterized by electronic transition(s) to an excited state in which a partial transfer of electronic charge from the donor to the acceptor moiety occurs [1]. The extensive study of charge transfer complexes (CT complexes) is due to their unique physical and chemical properties and the possibility of their application in various areas, such as organic semiconductors and solar cells [2–6], optoelectronics and optical communications [7,8], as well as pharmacology (antibacterial and anti-inflammatory activity) [9–12]. Organic semiconductors based on the CT complexes possess a number of attractive properties. First, obtaining heterostructures including donor and acceptor molecules makes it possible to design organic semiconductors with specified properties from a combination of existing molecules, reducing or eliminating the complexity of organic synthesis [6]. Second, the growth of the CT complex crystals is characterized by the realization of a long-range molecular order, the absence of grain boundaries, and a low amount of impurities and defects [13]. Third, it is the ability to exhibit ambipolar properties [14]. For these reasons, they are used as elements of organic electronics—OFETs, OLETs, and OLEDs [14,15].

Amino-substituted benzenes are often used as donors, and *p*-quinone derivatives are used as acceptors [7,10,14,16]. However, the formation of the CT complexes of *o*-quinones with amine derivatives is virtually not described in the literature. This is probably due to the instability of aniline-*o*-quinone charge transfer complexes and their rapid subsequent transformation into the corresponding quinonimines, phenoxazines [17–19] and other heterocyclic compounds [20]. The formation of the CT complexes as intermediate products in the reactions of 3,5-diamino-4-arylazopyrazoles and nitroalkanes with *o*-quinones is discussed in literature [21,22]; however, these complexes were not obtained in pure form. The existence of the CT complex in solution was postulated on the basis of spectrophotometric studies

* Corresponding author.
E-mail address: aled@ipoc.sfedu.ru (A.D. Dubonosov).

https://doi.org/10.1016/j.mtchem.2021.100462

and investigation of fluorescence quenching in the reaction of (4-dimethylaminobenzylidene)-(4,6-dimethylpyrimidine-2-yl) amine with *o*-chlor(brom)anil [23]. To date, the crystal forms of the CT complexes in the *o*-quinone series have not been described, and this area of chemistry remains virtually unexplored.

Thus, the search for new structural motifs in the design of charge transfer complexes with potentially useful physical and chemical properties represents a very urgent task. For this reason, we directed this work to the synthesis of a new type of *o*-quinone complex based on [1,10]-phenanthroline-5,6-dione (PD) and the investigation of its structure and properties using ^{1}H NMR, FTIR, UV–vis spectroscopy and elemental analysis, as well as X-ray diffraction, thermogravimetric (TG) and differential thermogravimetric (DTG) studies and density functional theory (DFT) quantum chemical calculations.

2. Results and discussion

2.1. Synthesis

Herein, we report on the study of the reaction between *p*-nitroaniline (PNA) and PD. The reaction of 9,10-phenanthren quinone with PNA leads to the corresponding 9,10-bisqui nonimine [24]. However, we have found that the interaction of PNA with PD in ethanol in mild conditions leads exclusively to a molecular PNA_3-PD_2 CT complex in a ratio of 3:2 (Scheme 1). The next stage of interaction, the formation of [1,10]-phenanthroline-5,6-dimine, was not observed, although it seems that it can be carried out under more harsh reaction conditions.

The formation of the CT complex PNA_3-PD_2 occurs at any mole ratio of reagents PNA and PD; however, the maximum yield (72%) of the crystal complex was observed at a ratio of 3 mol of PNA and 2 mol of PD.

The emergence of the CT complex PNA_3-PD_2 is accompanied by a change in the solution color during mixing of solutions PNA and PD and the subsequent formation of a bright red precipitate from the cooled reaction mixture. The crystals of the CT complex PNA_3-PD_2 are deeply colored, which is the result of the formation of new electronic absorption bands. Fig. 1 demonstrates that initial compounds PNA and PD are yellow, while the resulting crystals of the CT complex are dark maroon.

The diffuse reflectance UV–vis spectra of crystal powders of PNA, PD, and the CT complex PNA_3-PD_2 in the range of 300–650 nm obtained using the Kubelka-Munk function are shown in Fig. 2.

The long-wavelength absorption band of PD is characterized by a maximum at 417 nm and shoulders at 391 and 437 nm (Table 1). The short-wavelength absorption band has a maximum at 325 nm. Long-wavelength absorption of PNA is represented by a low-intensity band with a maximum at 498 nm and a shoulder at 514 nm, and the two short-wavelength bands have maxima at 343 and 397 nm. The absorption of solid CT complex PNA_3-PD_2 has one pronounced maximum at 393 nm, while the intense weakly structured long-wavelength absorption band extends up to 650 nm. This absorption, which is absent in PNA and in PD, is characteristic of charge transfer bands in the CT complex.

The electronic absorption spectra of the CT complex PNA_3-PD_2 solutions are characterized by long-wavelength absorption bands with maxima at 343–389 nm depending on the solvent (Table 1 and Fig. S1; Supplementary data). The bathochromic shift of the long-wavelength band in the absorption spectrum of complex PNA_3-PD_2 from toluene to DMSO occurs symbatically with changes in the long-wavelength absorption maximum of PNA. The short-wavelength absorption band of the CT complex PNA_3-PD_2 solutions has a maximum at 251–258 nm and shoulders at 292–295 and 301–306 nm. Analysis of the spectra shows that the absorption spectrum of the CT complex PNA_3-PD_2 solution represents the cumulative absorption spectrum of its constituent components PNA and PD in all solvents (Fig. S2, Supplementary data). Mixing of solutions of donor PNA and acceptor PD in different molar ratios does not cause spectral changes characteristic of charge transfer in solution (Fig. S3, Supplementary data). It should be assumed that solvation of the CT complex PNA_3-PD_2 leads to inhibition of the charge transfer process and dissociation of the complex to the initial components PNA and PD.

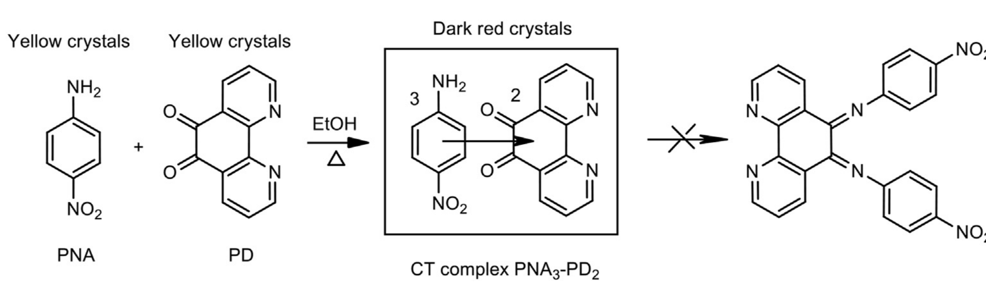

Scheme 1. Reaction of *p*-nitroaniline (PNA) with [1,10]-phenanthroline-5,6-dione (PD) in ethanol.

Fig. 1. Photos of the donor PNA (**A**), acceptor PD (**B**) and the resulting PNA_3-PD_2 complex (**C**).

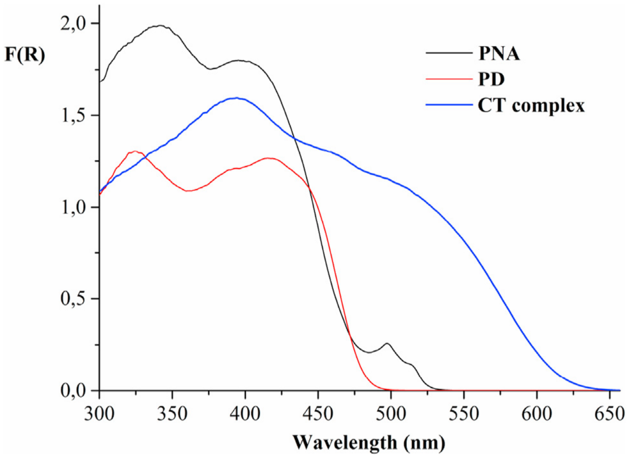

Fig. 2. Diffuse reflectance UV–vis spectra for PNA, PD, and the CT complex PNA_3-PD_2 (plotted in the form of Kubelka–Munk functions).

Table 1
UV–vis data for PNA, PD, and the CT complex PNA_3-PD_2 in the solid state and solutions.

	Absorption, λ_{max} (nm)		
	PNA	PD	PNA_3-PD_2
Solid state	498, 514^{sh}, 397	417, 437^{sh}, 391^{sh}, 325	393, 484^{sh}
Solvent			
Toluene	343	–[a]	343
Chloroform	348	–[a]	348, 258, 252^{sh}
MeCN	364	306^{sh}, 295^{sh}, 255	364, 306^{sh}, 295^{sh}, 255
THF	364	301^{sh}, 292^{sh}, 251	365, 301^{sh}, 292^{sh}, 251^{sh}
MeOH	371, 229	305^{sh}, 293^{sh}, 250, 235	370, 305, 295, 249^{sh}, 233
DMSO	389	306, 294	389, 306, 294

[a] Poorly soluble.

2.2. Crystal structure

The molecular structure of the CT complex PNA_3-PD_2 is shown in Fig. 3.

The crystal system of a single-crystal PNA_3-PD_2 is monoclinic with the space group $P2_1$. Unit cell parameters were measured at 293 K, unit cell volume is equal to 1815.93(3) Å^3 with a molecular mass of 834.76. The formation of a stable CT complex PNA_3-PD_2 is realized through hydrogen and donor-acceptor bonds of PNA with PD. In the crystal packing, complex forms voluminous coordination polymer tapes with a width of 25 Å and a thickness of ~2 Å (Figs. 4 and 5) because of the formation of extensive intermolecular hydrogen bonds involving PNA donor NH_2 fragment and the acceptor oxygen atoms of the nitro and carbonyl groups, as well as PD pyridine nitrogen atom. The interlayer distance between the planes of PD and PNA in adjacent layers is 3.4 Å. The smallest contact (2.801 Å) occurs between the nitrogen atom of the PNA amino group and the plane of the pyridine fragment of PD (Fig. 5). Shortest intermolecular nonbonding contacts are as follows: N82…C63 (2.88 Å); N82…C85 (2.99 Å); N84…C4 (2.88 Å); N84…C62 (2.92 Å); C6…C63 (3.08 Å); C62…C86 (3.08 Å).

In the ^1H NMR spectrum of complex PNA_3-PD_2, the proton signals of the donor PNA and acceptor PD parts correlate with each other in a 3:2 ratio, which corresponds to the composition of the complex established by X-ray diffraction study (Fig. S4, Supplementary data).

2.3. Thermal measurements

TG and DTG studies for PNA, PD, and the CT complex PNA_3-PD_2 were carried out under a nitrogen gas flow within a temperature range of 30–950 °C (Fig. 6, Table 2). The thermal decomposition of PNA is characterized by one very strong peak at 285 °C with a total

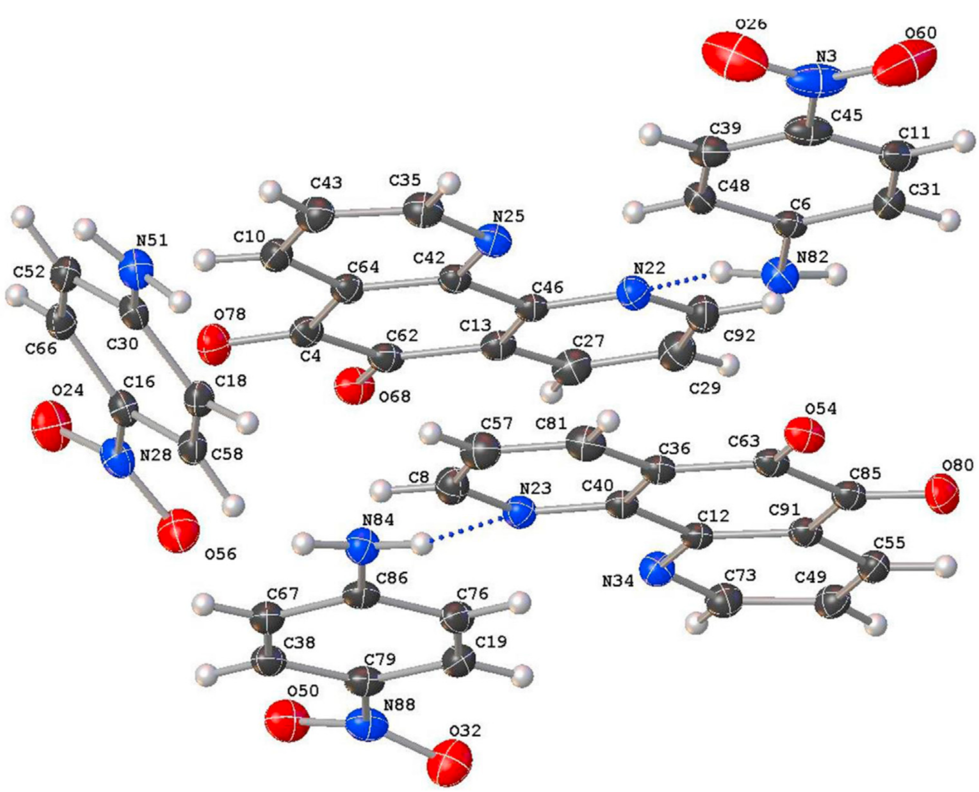

Fig. 3. The molecular structure of the CT complex PNA_3-PD_2. Unit cell parameters of the crystals, three-dimensional sets of intensities, and basic experimental and crystallographic data for the CT complex PNA_3-PD_2 are shown in Table S1 (Supplementary data). Full lists of bond lengths and bond angles are shown in Table S2 (Supplementary data).

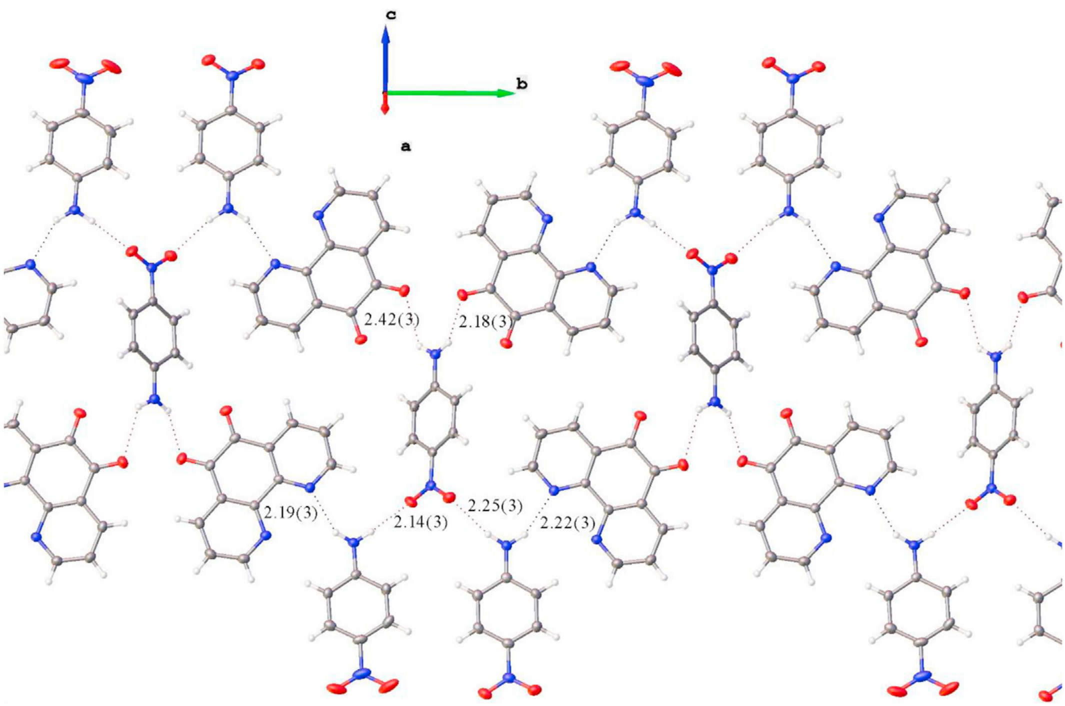

Fig. 4. Crystal packing in the structure of the CT complex PNA_3-PD_2. A fragment of a single-layer structural polymer elongated along the direction of the b axis (values of the lengths of hydrogen bonds are given). The intermolecular hydrogen bonds are indicated by dotted lines.

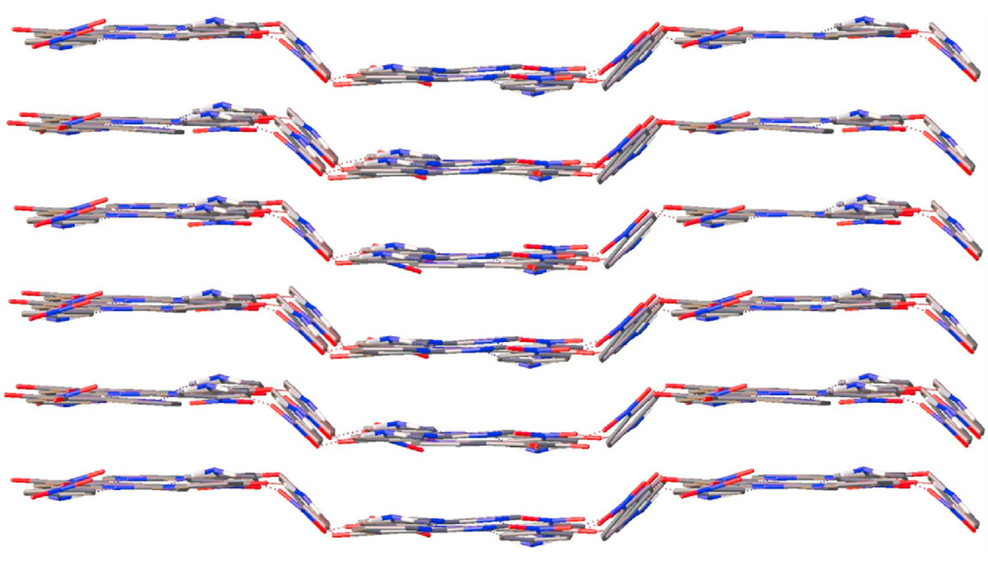

Fig. 5. Fragment of the layered structure of the CT complex PNA_3-PD_2.

mass loss of 100%, while PD shows two stages of decomposition at 347 °C and 734 °C with a mass loss of 70% and 30%, respectively. The CT complex PNA_3-PD_2 also decomposes in two degradation stages—at 260 °C and 740 °C with a mass loss of 37% and 63%, respectively. Differential scanning calorimetry (DSC) data for the PNA_3-PD_2, PD, and PNA are shown in Fig. S5 (Supplementary data).

2.4. Theoretical modeling

Optimization of the molecular structure of the CT complex PNA_3-PD_2 was carried out within the framework of the approximation of the density functional theory implemented in the BAND module of the AMS software package (Amsterdam Modeling Suite). The results of quantum chemical calculations of the CT complex PNA_3-PD_2 are in good agreement with the data of X-ray diffraction study (Fig. 7).

The CT complex PNA_3-PD_2 consists of two types of molecules—PNA and PD; however, in the crystal structure, the environment of individual molecules PNA and PD is different. PNA is characterized by three nonequivalent positions, while PD has two nonequivalent positions (Fig. 7**A**). The examination of the single layer of the complex (Fig. 7**B**) shows that most of the molecules lie in the layer plane, but there exist molecules PNA that come out of the layer plane—'PNA-out-of-plane' (Fig. 7**B** and **C**—highlighted in white). For

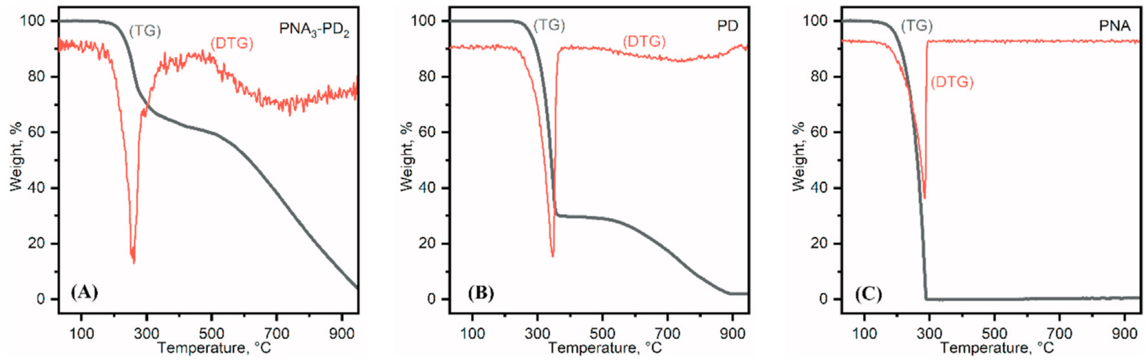

Fig. 6. Thermograms of PNA_3-PD_2 (A), PD (B), and PNA (C) samples.

Table 2
Thermal decomposition data for PNA, PD, and the CT complex PNA_3-PD_2.

Compound	DTG max, °C	TG%, mass loss
PNA	285	100
PD	347	70
	734	30
PNA_3-PD_2	260	37
	740	63

this nonequivalent position, the environment of molecule PNA differs significantly from the others. One of the hydrogen atoms of the 'PNA-out-of-plane' amino group is almost equidistant from the two oxygen atoms of the 'PD-sym' quinone group (highlighted in orange) at distances of 2.423 and 2.458 Å (Fig. 7**D**). The second hydrogen atom of the 'PNA-out-of-plane' amino group is characterized by an asymmetric arrangement of the nearest oxygen atoms of the 'PD-asym' quinone group (Fig. 7**D**, highlighted in red), which are located at distances of 2.181 and 2.500 Å. The oxygen atoms of the 'PNA-out-of-plane' nitro group are pairwise bound to the hydrogen atoms of the other two nonequivalent PNA positions with characteristic distances of 2.135 and 2.249 Å for the 'PNA-in-of-plane-PNA' and the 'PNA-in-of-plane-PD', respectively (Fig. 7**D**). At the same time, the second hydrogen atoms of the two nonequivalent positions of PNA are bound to the PD pyridine nitrogen atoms at a distance of 2.188 and 2.218 Å, respectively (Fig. 7**D**).

The experimental and calculated IR spectra of PNA, PD, and the CT complex PNA_3-PD_2 are shown in Figs. 8 and 9 and in Figs. S6–S10 (Supplementary data). Infrared wave numbers and tentative band assignments for PNA, PD, and PNA_3-PD_2 are shown in Table 3.

The IR spectrum of the CT complex PNA_3-PD_2 includes all main absorption bands of PNA and PD. Examination of the 1800-500 cm^{-1} region did not show additional peaks; however, the nature of all peaks in the IR spectrum for PNA_3-PD_2 was established by comparing the experimental spectra of PNA, PD, and CT complex PNA_3-PD_2 and theoretical calculations for PNA and PD. In the region of hydrogen atom vibrations, the splitting of the peaks of PNA amino group vibrations in the region of 3300–3500 cm^{-1} is noticeable, as well as the appearance of a new peak at 3185 cm^1. Calculations of the IR spectrum for PNA in the DFT approximation

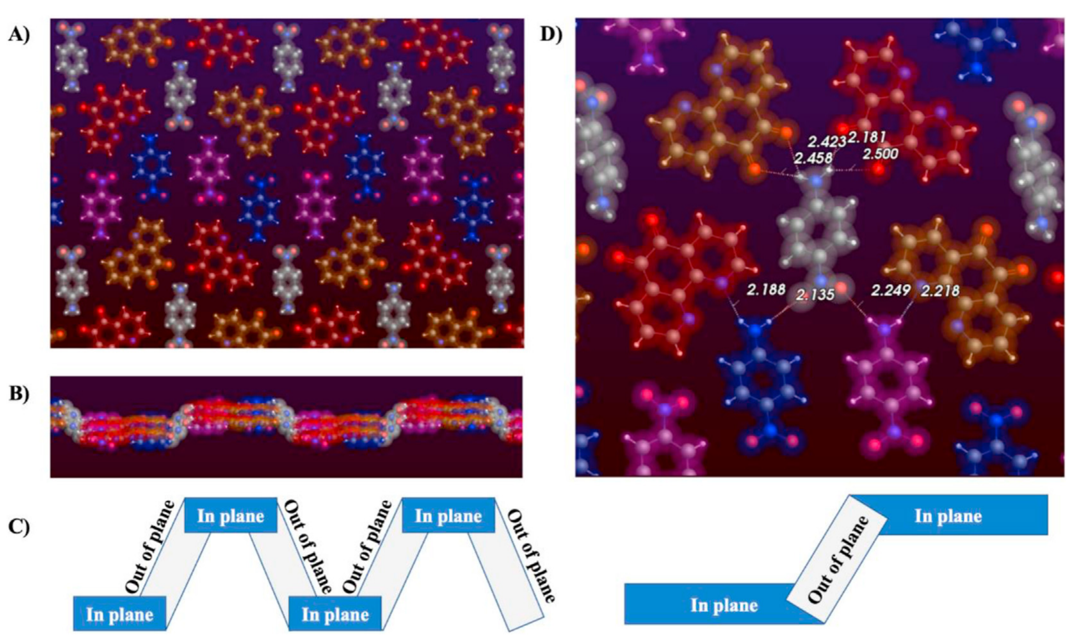

Fig. 7. Nonequivalent positions of molecules PNA and PD in the structure of the CT complex PNA_3-PD_2. Position 'PNA-out-of-plane' is highlighted in white, 'PNA-in-of-plane-PNA' in blue, 'PNA-in-of-plane-PD' in purple, 'PD-asym' in red, 'PD-sym' in orange. (**A**) Projection onto the CT complex monolayer perpendicular to the monolayer plane. (**B**) Projection onto the CT complex monolayer along the monolayer plane. (**C**) Schematic representation of 'in-plane' and 'out-of-plane' parts. (**D**) Local structure of nonequivalent 'PNA-out-of-plane' position.

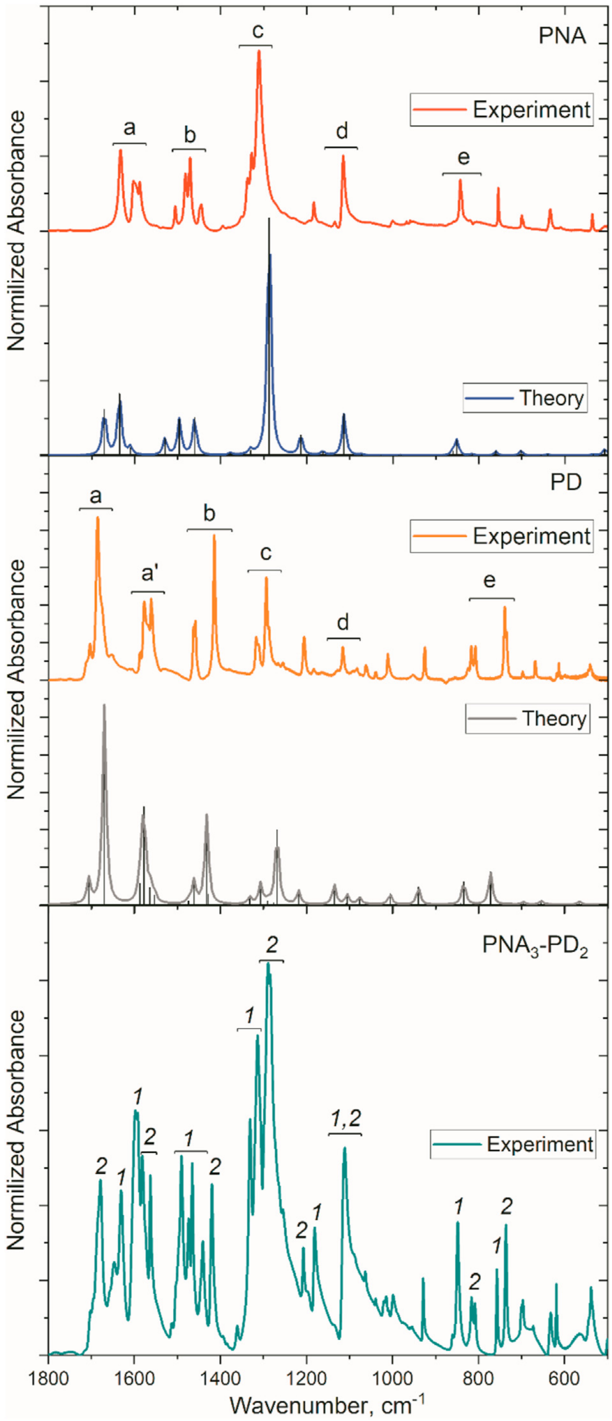

Fig. 8. Experimental and DFT-calculated IR spectra of PNA, PD, and the CT complex PNA$_3$-PD$_2$ in the fingerprint region.

indicate that the peaks in the region of 3482 and 3363 cm^{-1} reflect symmetric and asymmetric vibrations of the amino group, respectively. Therefore, the splitting of the peaks of symmetric and asymmetric vibrations can be caused by different environments in 'PNA-in-of-plane' and 'PNA-out-of-plane' positions. The appearance of an intense peak at 3185 cm^{-1} may be associated with C—H vibrations.

Splitting of the absorption bands of NH-group vibrations and the appearance of a new absorption band of CH-groups in the IR spectrum of the CT complex PNA$_3$-PD$_2$ confirms the presence of intermolecular interactions between the initial compounds PNA and PD, in particular, the implementation of donor-acceptor bonds of the amino group NH$_2$ with the nitro group of PNA, carbonyl groups, and heterocyclic nitrogen atoms of PD.

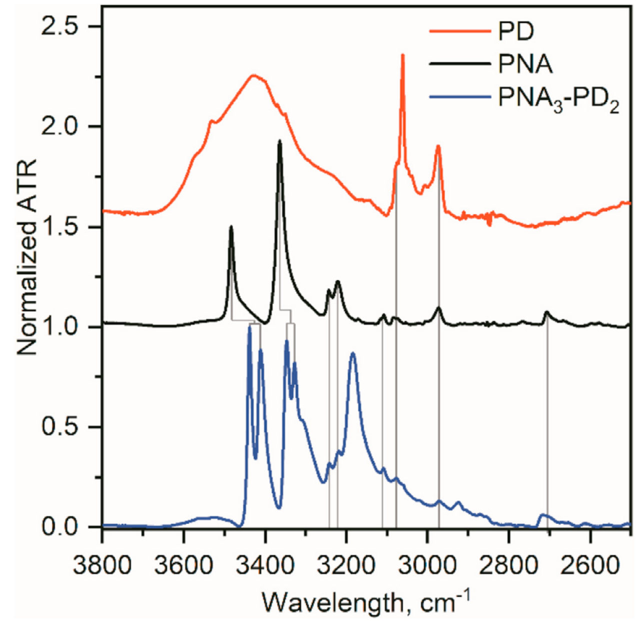

Fig. 9. Experimental IR spectra of PNA, PD, and the CT complex PNA$_3$-PD$_2$ in the region of hydrogen atom vibrations.

Table 3
Infrared wave numbers[a] and tentative band assignments for PNA, PD, and PNA$_3$-PD$_2$.

PNA	PD	PNA$_3$-PD$_2$	Assignments
3482s		3438s, 3411s	ν(NH$_2$) *asym*; PNA
	3429s, br		ν(H$_2$O)
3363s		3350s, 3328s, 3305w	ν(NH$_2$) *sym*; PNA
3244m		3244m	ν(C—H); aromatic, PNA
3222m		3222m	ν(C—H); aromatic, PNA
		3185s	ν(C—H); intermolecular
3078w	3078w	3078w	ν(C—H); aromatic PNA, PD
2974w	2974s	2974w	ν(C—H); aromatic PNA
	1705m, 1686s	1679s	ν(C=O); PD
1632s		1630s	ν(NH$_2$) *sym* PNA
1601s		1597s	ν(C=C); aromatic PNA
	1577s	1580m	ν(C=C); PD
	1558s	1562m	ν(C=C); PD
1505m		1490s	PNA
1482s		1475m	PNA
1471s	1461s	1465m	PNA, PD
1446m		1442m	PNA
	1415s	1419s	PD
1326w		1331s	NH$_2$; PNA
1312s		1313s	NO$_2$; PNA
	1293s	1288s	PD
1182m		1180m	PNA
	1116	1110s	PD
1114s			PNA
843s		848s	PNA wagging
	813m	814m	PD wagging
755s		758m	PNA twisting
	738s	737s	PD twisting
700w		698m	PNA twisting
634m		632m	PNA
536m		539m	PNA

[a] m, medium; s, strong; w, weak; br, broad.

To assess the presence of semiconductor properties of complex PNA_3-PD_2, quantum chemical calculations of the band gap were carried out (Fig. 10). The structure was calculated within the framework of density functional theory using the BAND software package. Analytical energy gradients for systems with translational invariance were formulated within the framework of Kohn-Sham density functional theory. Energy gradients were implemented in the BAND program, which directly used a basic set of Bloch functions consisting of numerically calculated atomic orbitals and Slater-type orbitals. When developing the calculation procedure, we carried out calculations using exchange-correlation functionals of various types. In particular, we used the local electronic density approximation. In this approach, the one-determinant electron wave function was represented in the form of a linear combination of basic functions centered at atoms. Other classes of tested exchange-correlation functionals include the approximation of generalized gradients (GGA: PBE, BLYP) and approximation of range-separated functionals. The basis set consisted of atomic orbitals obtained by numerically calculating the Kohn-Sham equations for isolated spherical atoms, supplemented with a set of Slater orbitals. We tested various basis sets of Slater functions: the DZ type (two-exponent atomic orbitals), the DZP type (two-exponent atomic orbitals with addition of polarization function), and the TZP type (three-exponent atomic orbitals with addition of polarization function). Different dimensions of the 'frozen' core or a number of core orbitals were tested additionally. In this approach, the core orbitals of each element were calculated for a solitary atom once and were fixed in further calculations.

Calculations of the electronic structure showed that the CT complex PNA_3-PD_2 is a straight-band semiconductor with a band gap of 2.11 eV.

3. Experimental

3.1. Materials and instrumentation

PNA (98%, Alfa Aesar) was used as the starting reagent. PD was obtained using the known method [25]. Toluene, chloroform, THF, acetonitrile, methanol, and DMSO of spectroscopic grade (Aldrich) were used to prepare solutions. The ^{1}H NMR spectrum was obtained using Bruker AVANCE 600 spectrometer, the signals were referred with respect to the signals of residual protons of deutero solvent. The FTIR spectra were measured on a Bruker Vertex 70 spectrometer in transmission geometry. There were total 256 scans per sample obtained with a 0.5-cm^{-1} resolution. The UV–Vis diffuse reflectance spectra were recorded on an UV–Vis Shimadzu UV2600 equipped with ISR2600Plus integration sphere. The elemental analysis was carried out on the automatic CHNS analyzer 'Euro EA-3000' (Euro Vector) in the Joint Research Center PMR IGIC RAS. TG and DSC measurements were carried out under a nitrogen gas flow within a temperature range of 30–950 °C and the heating rate 10 C/min using Netzsch STA 449 F5 Jupiter system. Melting points were determined on a Fisher-Johns apparatus. NMR and IR spectra were recorded on the equipment of the Center for Collective Usage 'Molecular spectroscopy' of the Southern Federal University.

3.2. Synthesis of the CT complex PNA_3-PD_2

The concentrated solutions of PD (2 mmol, 0.42 g) in EtOH (30 mL) and PNA (3 mmol, 0.414 g) in EtOH (20 mL) were mixed by heating. The solvent was evaporated to a volume of 10 mL. After cooling at room temperature, the red precipitate of PNA_3-PD_2 was filtered off and rinsed with ethanol (5 mL). Yield of PNA_3-PD_2 was

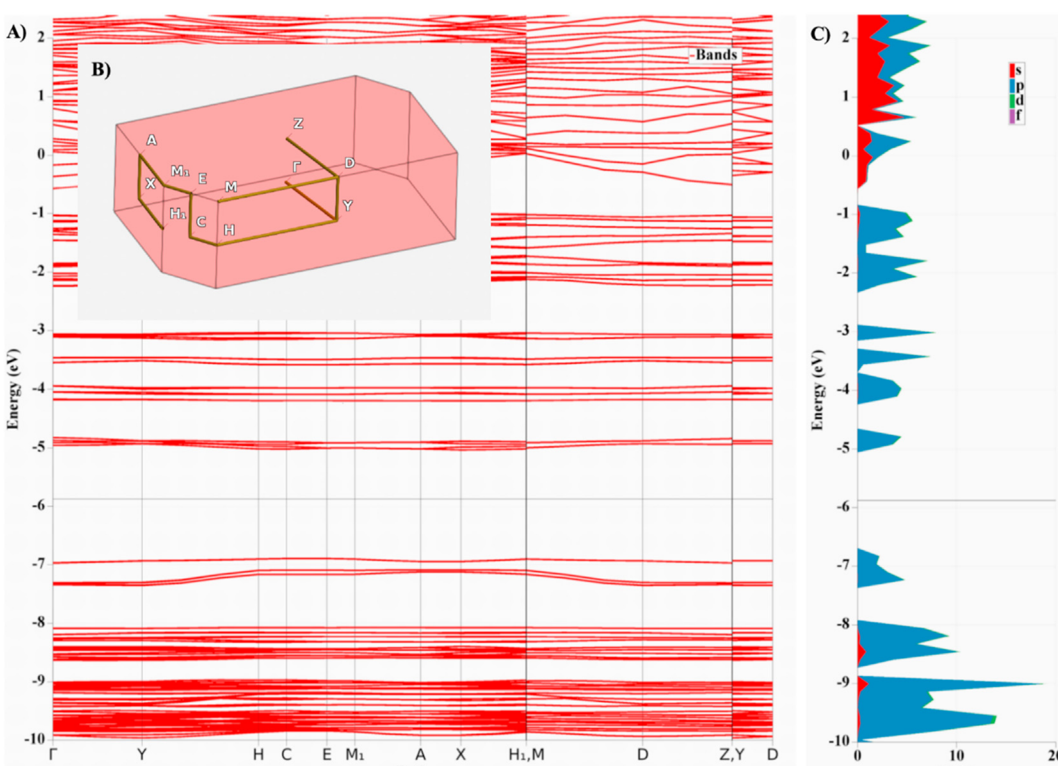

Fig. 10. (A) Band structure calculation for the CT complex PNA_3-PD_2 for the standard monoclinic cell path (B). (**C**) Cumulative density of states for the CT complex PNA_3-PD_2.

0.60 g (72%). By concentrating the mother liquor, an additional amount of the CT complex PNA_3-PD_2 can be obtained. Red crystals, mp 153 °C (ethanol). IR ν_{max} (cm^{-1}): 3438, 3411, 3350, 3328, 3305, 3244, 3222, 3185, 3078, 2974, 1679, 1630, 1597, 1580, 1562, 1490, 1475, 1465, 1442, 1419, 1331, 1313, 1288, 1180, 1110, 848, 814, 758, 737, 698, 632, 539. ^{1}H NMR (600 MHz, $CDCl_3$) δ (ppm): 6.59 (d, 3H, arom. H_{amine}, J = 9.0 Hz), 6.67 (s, 3H, H_{NH2}), 7.66 (t, 2H, arom. $H_{quinone}$, J = 6.0 Hz), 7.93 (d, 3H, arom. H_{amine}, J = 9.0 Hz), 8.38 (d, 2H, arom. $H_{quinone}$, J = 6.0 Hz), 8.98 (d, 2H, arom. $H_{quinone}$, J = 6.0 Hz). Calcd. for $C_{42}H_{30}N_{10}O_{10}$ (%): C, 60.43; H, 3.62; N, 16.78. Found (%): C, 60.24; H, 3.68; N, 16.51.

3.3. X-ray diffraction study

Crystals of PNA_3-PD_2 suitable for X-ray structural analysis were obtained by slow evaporation of an ethanol solution at room temperature. X-ray structural studies were performed on an Agilent SuperNova diffractometer using a microfocus X-ray source with copper anode and an Atlas S2 CCD detector. Monocrystals of $C_{42}H_{30}N_{10}O_{10}$ (M = 834.76 g/mol) are monoclinic: a = 7.33940(10) Å, b = 23.3638(2) Å, c = 10.78820(10) Å, β = 101.0000(10), V = 1815.93(3) Å^3, Z = 2, T = 100.01(10) K, μ(CuKα) = 0.943 mm^{-1}, D_{calc} = 1.527 g/cm^3, space group P2_1 (no. 4). 34,196 Reflections were measured (7.568° ≤ 2Θ ≤ 147.864°), 7245 unique (R_{int} = 0.0262, R_{sigma} = 0.0172) which were used in all calculations. The final R_1 was 0.0275 (I > 2σ(I)), and wR_2 was 0.0741 (all data). The collection of reflexes, determination, and refinement of unit cell parameters were performed by using the specialized CrysAlisPro 1.171.38.41 software suite [26]. The structures were solved by using ShelXT program [27], and structure refinement was also performed with ShelXL program [28]. Molecular graphics were rendered and prepared for publication with the Olex2 version 1.2.10 software suite [29]. The complete X-ray diffraction data sets were deposited at the Cambridge Crystallographic Data Center (CCDC 2041741).

3.4. Quantum chemical calculations

To clarify the structure of all compounds, geometric optimization was previously performed in the framework of the electron density functional theory by minimizing the total energy of the system (software package AMS) [30]. For molecules PNA and PD, calculations were performed in direct space using the exchange-correlation potential BLYP (the exchange part of Becke [31] with the LYP correction [32]) and the basic set TZP [33] implemented in the ADF software module [34]. To calculate the IR spectra for PNA and PD, the vibrational frequencies were calculated using the analytical solution of the Kohn-Sham equation in the framework of perturbation theory [35–37]. The calculated frequencies were multiplied by a factor of 1.037 for comparison with the experimental spectra, and the spectral broadening was reproduced by calculating the convolution of the intensities of the calculated peaks from the Lorentz functions (with a full width at half-height of 15 cm^{-1}). Calculations of the band structure and band gap of the CT complex PNA_3-PD_2 were performed in the approximation for periodic systems implemented in the BAND module [38,39] of the AMS software package. The spatially separated hybrid exchange-correlation potential HSE06 [40] and the base set TZP [33] were used to correctly describe the band gap.

4. Conclusions

To sum up, the first stable CT complex in *o*-quinone series in the crystal state was obtained by the reaction of PNA with PD. The obtained complex represents a first example of an isolated intermediate in the condensation reaction of *o*-quinones with anilines, usually resulting in the formation of the corresponding quinonimines. The structure of the PNA_3-PD_2 complex was determined by X-ray diffraction studies, which showed that the ratio of donor (PNA) and acceptor (PD) is 3:2. IR spectroscopy and quantum chemical calculations have shown the implementation of several types of donor-acceptor bonds of the PNA amino group with the nitro group of another PNA molecule, PD carbonyl groups, and heterocyclic nitrogen atoms. The diffuse reflectance spectrum of the crystalline powder of the CT complex PNA_3-PD_2 is characterized by a long-wavelength weakly structured absorption band up to 650 nm, which is typical for the CT complex. The CT complex PNA_3-PD_2 is stable only in the solid state; when it is dissolved in solvents of different polarities, dissociation into the initial donor and acceptor molecules is observed. According to the data of quantum chemical calculations, the resulting complex PNA_3-PD_2 has the properties of direct-gap semiconductors.

CRediT authorship contribution statement

E.A. Gusakov: Investigation, Validation. **O.P. Demidov:** Investigation. **I.O. Tupaeva:** Investigation. **E.V. Vetrova:** Investigation. **M.A. Soldatov:** Investigation, Formal analysis, Methodology. **A.A. Tereshchenko:** Investigation, Software. **A.D. Dubonosov:** Formal analysis, Data curation, Writing – review & editing. **Y.A. Sayapin:** Conceptualization, Methodology, Writing – review & editing. **A.V. Metelitsa:** Supervision, Conceptualization. **V.I. Minkin:** Supervision.

Declaration of competing interest

The authors declare that they have no known competing financial interests or personal relationships that could have appeared to influence the work reported in this paper.

Acknowledgements

Yu. A. Sayapin and A.D. Dubonosov worked within the framework of the State Assignment of Southern Scientific Centre of RAS No. 01201354239. V. I. Minkin and E. A. Gusakov worked under the financial support of the Ministry of Science and Higher Education of the Russian Federation (the State Assignment in the field of scientific activity No. BAZ0110/20-3-09IKh).

Appendix A. Supplementary data

Supplementary data to this article can be found online at https://doi.org/10.1016/j.mtchem.2021.100462.

References

[1] Glossary of terms used in physical organic chemistry (IUPAC Recommendations 1994), Pure Appl. Chem. 66 (1994) 1077–1184, https://doi.org/10.1351/pac199466051077.
[2] G. Saito, Y. Yoshida, Development of conductive organic molecular assemblies: organic metals, superconductors, and exotic functional materials, Bull. Chem. Soc. Jpn. 80 (1) (2007) 1–137, https://doi.org/10.1246/bcsj.80.1.
[3] H. Bai, Y. Wang, P. Cheng, Y. Li, D. Zhu, X. Zhan, Acceptor–donor–acceptor small molecules based on indacenodithiophene for efficient organic solar cells, ACS Appl. Mater. Interfaces 6 (11) (2014) 8426–8433, https://doi.org/10.1021/am501316y.
[4] T.-W. Ng, M.-F. Lo, M.-K. Fung, W.-J. Zhang, C.-S. Lee, Charge-transfer complexes and their role in exciplex emission and near-infrared photovoltaics, Adv. Mater. 26 (2014), https://doi.org/10.1002/adma.201400563, 5226–5226.
[5] J. Heiska, M. Nisula, M. Karppinen, Organic electrode materials with solid-state battery technology, J. Mater. Chem. A 7 (32) (2019) 18735–18758, https://doi.org/10.1039/C9TA04328D.
[6] J. Zhang, W. Xu, P. Sheng, G. Zhao, D. Zhu, Organic donor–acceptor complexes as novel organic semiconductors, Acc. Chem. Res. 50 (7) (2017) 1654–1662, https://doi.org/10.1021/acs.accounts.7b00124.

[7] A. Mostafa, N. El-Ghossein, G.B. Cieslinski, H.S. Bazzi, UV–Vis, IR spectra and thermal studies of charge transfer complexes formed in the reaction of 4-benzylpiperidine with σ- and π-electron acceptors, J. Mol. Struct. 1054–1055 (2013) 199–208, https://doi.org/10.1016/j.molstruc.2013.09.007.

[8] F. Yakuphanoglu, M. Arslan, The fundamental absorption edge and optical constants of some charge transfer compounds, Opt. Mater. 27 (2004) 29–37, https://doi.org/10.1016/j.optmat.2004.01.017.

[9] A.A. El-Habeeb, F.A. Al-Saif, M.S. Refat, Charge transfer complex of some nervous and brain drugs – Part 1: synthesis, spectroscopic, analytical and biological studies on the reaction between haloperidol antipsychotic drugs with π-acceptors, J. Mol. Struct. 1034 (2013) 1–18, https://doi.org/10.1016/j.molstruc.2012.08.045.

[10] Zulkarnain, I.M. Khan, A. Ahmad, L. Miyan, M. Ahmad, N. Azizc, Synthesis of charge transfer complex of chloranilic acid as acceptor with p-nitroaniline as donor: crystallographic, UV–visible spectrophotometric and antimicrobial studies, J. Mol. Struct. 1141 (2017) 687–697, https://doi.org/10.1016/j.molstruc.2017.03.050.

[11] S.A. Gaballa, A.S. Amin, Preparation, spectroscopic and antibacterial studies on charge-transfer complexes of 2-hydroxypyridine with picric acid and 7,7′,8,8′-tetracyano-*p*-quinodimethane, Spectrochim. Acta A 145 (2015) 302–312, https://doi.org/10.1016/j.saa.2015.03.005.

[12] H. Duymus, M. Arslan, M. Kucukislamoglu, M. Zengin, Charge transfer complex studies between some non-steroidal anti-inflammatory drugs and π-electron acceptors, Spectrochim. Acta A 65 (2006) 1120–1124, https://doi.org/10.1016/j.saa.2006.01.044.

[13] X. Zhang, H. Dong, W. Hu, Organic semiconductor single crystals for electronics and photonics, Adv. Mater. 30 (44) (2018), https://doi.org/10.1002/adma.201801048. Article 1801048.

[14] K.P. Goetz, D. Vermeulen, M.E. Payne, C. Kloc, L.E. McNeil, O.D. Jurchescu, Charge-transfer complexes: new perspectives on an old class of compounds, J. Mater. Chem. C 2 (17) (2014) 3065–3076, https://doi.org/10.1039/C3TC32062F.

[15] T. Higashino, M. Dogishi, T. Kadoya, R. Sato, T. Kawamoto, T. Mori, Air-stable n-channel organic field-effect transistors based on charge-transfer complexes including dimethoxybenzothienobenzothiophene and tetracyanoquinodimethane derivatives, J. Mater. Chem. C 4 (2016) 5981–5987, https://doi.org/10.1039/C6TC01532H.

[16] S. Shao, Y. Guo, L. He, S. Jiang, X. Yu, New non-covalent charge–transfer complex of calix[4]pyrrole–chloranil: as a potential colorimetric anion sensor, Tetrahedron Lett. 44 (10) (2003) 2175–2178, https://doi.org/10.1016/S0040-4039(03)00154-0.

[17] V.I. Simakov, S.V. Kurbatov, O.Ya. Borbulevych, M.Yu. Antipin, L.P. Olekhnovich, Structures of condensation products of ortho-aminophenols with ninhydrin, Russ. Chem. Bull. 50 (6) (2001), https://doi.org/10.1023/A:1011333722238, 1064–1064.

[18] G.A. Abakumov, N.O. Druzhkov, Yu.A. Kurskii, A.S. Shavyrin, NMR study of products of thermal transformation of substituted *N*-aryl-*o*-quinoneimines, Russ. Chem. Bull. 52 (3) (2003) 712–717, https://doi.org/10.1023/A:1023979311368.

[19] G.A. Abakumov, N.O. Druzhkov, Yu.A. Kurskii, L.G. Abakumova, A.S. Shavyrin, G.K. Fukin, A.I. Poddelskii, V.K. Cherkasov, L.S. Okhlopkova, Quinone imines and aminophenols as precursors of new heterocycles, Russ. Chem. Bull. 54 (11) (2005) 2571–2577, https://doi.org/10.1007/s11172-006-0157-7.

[20] V.V. Tkachev, G.V. Shilov, S.M. Aldoshin, Yu.A. Sayapin, Nghia Bang Duong, V.N. Komissarov, V.I. Minkin, Synthesis and structure of *7H*-12-Oxa-3,7-diazapleiadenes, Russ. J. Org. Chem. 47 (9) (2011) 1329–1334, https://doi.org/10.1134/S1070428011090120.

[21] A.A. Hassan, N.K. Mohamed, A.A. Aly, A.-F.E. Mourad, Reactions of 3,5-diamino-4-arylazopyrazoles with chlorinated quinones, Bull. Soc. Chim. Belg. 105 (4) (1996) 159–162, https://doi.org/10.1002/bscb.19961050403.

[22] Sh. Itoh, J. Maruta, Sh. Fukuzumi, Addition–cyclization reaction of nitroalkane anions with *o*-quinone derivatives *via* electron transfer in the charge-transfer complexes, J. Chem. Soc., Perkin Trans. 2 (1996) 1429–1433, https://doi.org/10.1039/P29960001429.

[23] Y.S. El-Sayed, Spectrophotometric and fluorescence quenching studies of the charge transfer complexation of (4-dimethylamino-benzylidene)-(4,6-dimethyl-pyrimidin-2-yl)-amine with some organic acceptors, Spectrochim. Acta A 78 (2011) 1227–1233, https://doi.org/10.1016/j.saa.2010.11.034.

[24] N. Raman, T.R. Arun, R. Mahalakshmi, S. Packianathan, R. Antony, Appraisal of DNA obligatory, DNA cleavage and in vitro anti-biogram efficiency of 9,10-phenanthrenequinone based metal complexes, Inorg. Chem. Commun. 46 (2014) 263–267, https://doi.org/10.1016/j.inoche.2014.06.011.

[25] F. Calderazzo, F. Marchetti, G. Pampaloni, V. Passarelli, Co-ordination properties of 1,10-phenanthroline-5,6-dione towards group 4 and 5 metals in low and high oxidation states, J. Chem. Soc., Dalton Trans. 24 (1999) 4389–4396, https://doi.org/10.1039/A906016B.

[26] CrysAlisPro, version 1.171.38.41, Rigaku Oxford Diffraction, 2015. https://www.rigaku.com/en/products/smc/crysalis.

[27] G.M. Sheldrick, *SHELXT* – integrated space-group and crystal-structure determination, Acta Crystallogr. A71 (2015) 3–8, https://doi.org/10.1107/S2053273314026370.

[28] G.M. Sheldrick, Crystal structure refinement with *SHELXL*, Acta Crystallogr. C71 (2015) 3–8, https://doi.org/10.1107/S2053229614024218.

[29] O.V. Dolomanov, L.J. Bourhis, R.J. Gildea, J.A.K. Howard, H. Puschmann, *OLEX2*: a complete structure solution, refinement and analysis program, J. Appl. Crystallogr. 42 (2009) 339–341, https://doi.org/10.1107/S0021889808042726.

[30] AMS 2019.3, SCM, Theoretical Chemistry, Vrije Universiteit, Amsterdam, The Netherlands, http://www.scm.com.

[31] A.D. Becke, Density-functional exchange-energy approximation with correct asymptotic behavior, Phys. Rev. A 38 (6) (1988) 3098–3100, https://doi.org/10.1103/PhysRevA.38.3098.

[32] C.T. Lee, W.T. Yang, R.G. Parr, Development of the Colle-Salvetti correlation-energy formula into a functional of the electron density, Phys. Rev. B 37 (2) (1988) 785–789, https://doi.org/10.1103/PhysRevB.37.785.

[33] E. van Lenthe, E.J. Baerends, Optimized Slater-type basis sets for the elements 1–118, J. Comput. Chem. 24 (9) (2003) 1142–1156, https://doi.org/10.1002/jcc.10255.

[34] G. te Velde, F.M. Bickelhaupt, E.J. Baerends, C. Fonseca Guerra, S.J.A. van Gisbergen, J.G. Snijders, T. Ziegler, Chemistry with ADF, J. Comput. Chem. 22 (9) (2001) 931–967, https://doi.org/10.1002/jcc.1056.

[35] S.K. Wolff, Analytical second derivatives in the Amsterdam density functional package, Int. J. Quant. Chem. 104 (5) (2005) 645–659, https://doi.org/10.1002/qua.20653.

[36] H. Jacobsen, A. Bérces, D.P. Swerhone, T. Ziegler, Analytic second derivatives of molecular energies: a density functional implementation, Comput. Phys. Commun. 100 (3) (1997) 263–276, https://doi.org/10.1016/S0010-4655(96)00119-1.

[37] A. Bérces, R.M. Dickson, L. Fan, H. Jacobsen, D. Swerhone, T. Ziegler, An implementation of the coupled perturbed Kohn-Sham equations: perturbation due to nuclear displacements, Comput. Phys. Commun. 100 (3) (1997) 247–262, https://doi.org/10.1016/S0010-4655(96)00120-8.

[38] G. te Velde, E.J. Baerends, Precise density-functional method for periodic structures, Phys. Rev. B 44 (15) (1991) 7888–7903, https://doi.org/10.1103/PhysRevB.44.7888.

[39] BAND2018, SCM, Theoretical Chemistry, Vrije Universiteit, Amsterdam, The Netherlands, http://www.scm.com.

[40] J. Heyd, G.E. Scuseria, M. Ernzerhof, Hybrid functionals based on a screened Coulomb potential, J. Chem. Phys. 118 (18) (2003) 8207–8215, https://doi.org/10.1063/1.1564060.